THE JOURNAL OF PHYSICAL CHEMISTRY C

Article

pubs.acs.org/JPCC

Knowledge Led Master Code Search for Atomic and Electronic Structures of LaF_3 Nanoclusters on Hybrid Rigid Ion–Shell Model–DFT Landscapes

Scott M. Woodley*

Kathleen Lonsdale Materials Chemistry, Department of Chemistry, University College London, 20 Gordon Street, London WC1H 0AJ, United Kingdom

ABSTRACT: Stable and metastable atomic configurations of stoichiometric $(LaF_3)_n$ nanoclusters are obtained for n = 1 to 6 using Monte Carlo global optimization techniques implemented in newly developed software. All configurations are refined using an all-electron DFT approach with the PBEsol exchange and correlation functional. To reduce the computational cost, approximate configurations were initially filtered out using a basin hopping algorithm that was biased toward finding either the global minimum or all metastable minima on the six energy landscapes defined by interatomic potentials within a polarizable shell model. In both algorithms, standard local optimization methods are employed to relax trial random atomic configurations whereby the polarization of the ions is initially constrained to improve convergence to local energy minima. The global optimization routines were implemented within the in-house Knowledge Led Master Code (KLMC). Electronic characterization of the refined structures included the calculation of vertical ionization potentials and electron affinities using the ΔSCF approach at the PBEsol DFT level and the many-body G_0W_0/PBEsol0 theory which employs the hybrid density functional initial guess of the quasi-particle orbitals. The atomic structure of the nanoclusters can be seen to evolve with size from a trigonal pyramid to ring structures and finally to compact symmetrical configurations, where the coordination of higher charged La gradually increases. Additional fluorine ions are accommodated between two La ions: single fluoride (−F−) bridges are replaced by bridge pairs or trios, although more than three fluoride bridges between two cations are heavily penalized in energy and cluster ranking. There is also a trend for the external surface of LaF_3 nanoclusters to be decorated by singly coordinated fluorine anions, one per outer La ion for larger nanoclusters. For the global minimum $(LaF_3)_n$ nanoclusters, although the changes are modest, the ionization potential decreases, and the electron affinity increases with n, effectively decreasing the precursor of the band gap of the bulk phase. The majority of the metastable nanoclusters follows this trend, with the exception of configurations with at least one exposed cation at the surface which is not terminated by an anion. These nanoclusters have a greater electron affinity that could be attributed to structural features analogous to defects in solids.

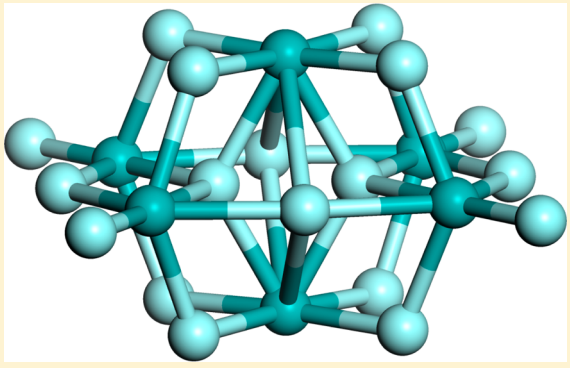

1. INTRODUCTION

Lanthanum fluoride has been reported as having one of the highest known ionic conductivities and is frequently used as a nonmagnetic host for spectroscopic investigations of paramagnetic lanthanide ions.[1] It has an anomalously high heat capacity (above 900 K),[2] is widely used in electrodes, and is found in other applications including fluorescent lamps, fiber optics, and radiation applications.[3] More generally, fluorides with the tysonite (LaF_3) structure are useful in optical applications like UV scintillators or solid-state lasers (see ref 4 and references therein). For rare earth doped fluoride materials, infrared to ultraviolet solid-state lasers are possible[5,6] and—in the sensitized-nanoparticle form—optical amplifiers.[7] More recently, nanoparticles of rare earth doped LaF_3 have been used to create white-emitting single phosphor for use in light-emitting diodes (LEDs).[8] As a thin film, LaF_3 has been investigated as a possible electrolyte for oxygen sensing.[9]

Driven in part by the wide-ranging applications of nanoparticulate materials in catalysis, electronics, and energy conversion, there is great interest in the synthesis and characterization of nanoclusters.[10,11] In this size regime both the properties and the atomic structure of the particles may differ significantly from that of the bulk phases.[12,13] Moreover, no clear diffraction patterns are obtainable, and structure determination from experiment is often highly problematic. Indeed, there has not yet appeared an experimental technique capable of reliable characterization of the local structure of nanoclusters, and thus elucidation of the structures and therefore the properties of nanoparticulate matter are fraught with difficulties.

Received: July 11, 2013
Revised: September 30, 2013
Published: October 2, 2013

   dx.doi.org/10.1021/jp406854j | J. Phys. Chem. C 2013, 117, 24003–24014

Typically it is assumed that the nanoclusters will adopt the configuration with the lowest energy of formation, or at least the atomic structure will resemble one or more of those in the set of low-energy stable and metastable configurations. Certain sized nanoclusters, either from laser ablation of a surface or from nucleation in solution, are sometimes more readily formed and are referred to in the literature as magic. Magic numbers, or preferred values of n, will depend not only on the stoichiometry but also on the compound. For example, if $(XY)_n$ nanoclusters are predicted (energetically more favorable) to form perfect cuboids cut from the NaCl rock salt phase, then usually there are many magic numbers, each corresponding to a size, value of n, where this is possible.[14−16] However, where simulations predict that the lowest energy $(XY)_n$ configuration for a compound is bubble-like, then mass spectra for synthesized nanoclusters of this compound typically have a smaller set of magic numbers; magic numbers either match the size where high symmetry (T_h, then T_d, and to a lesser extend T) is possible[17] or where a bulk-like or filled cage structure is a low energy configuration.[18−21]

A large number of global optimization schemes have been developed and applied to predicting the atomic structures of inorganic nanoclusters.[22−32] They have been applied to a range of compounds with different stoichiometry: there are plenty of examples of 1−1 compounds ($(AgI)_n$,[33] $(CdTe)_n$,[34] $(LiF)_n$,[27] $(MgO)_n$,[35,36] $(ZnO)_n$[37,38]...); as well as 1−2 compounds ($(MgF_2)_n$,[39−41] $(HfO_2)_n$,[42] $(SiO_2)_n$,[32] $(TiO_2)_n$,[43−47] $(ZrO_2)_n$[48]...); and also 2−3 compounds ($(Al_2O_3)_n$,[49−52] $(Ga_2O_3)_n$,[51,53] $(Ge_2S_3)_n$,[54] $(In_2O_3)_n$.[55]...). Here we are interested in an example of the less studied 1−3 compounds, namely, $(LaF_3)_n$—atomic configurations of which may be data-mined for other 1−3 compounds.

The aim of the work is to predict the global and lower energy metastable $(LaF_3)_n$ atomic structures for each value of n (1 to 6). Although for small nanoclusters it is possible to search the energy landscape defined by electronic structure (ES) methods, here the initial global search is for the local energy minima as defined by an atomistic method that employs analytical interatomic potentials (IPs) to describe the interaction between atoms (or ions). These lower energy atomic structures are subsequently refined using an electronic structure method. This multistage approach has two key advantages: energies on the IP landscape are far cheaper to compute, and the IP energy function is often more robust (no electronic structure to converge, which can be problematic for a trial cluster that contains at least one nonsensible interatomic distance). The former is particularly important for larger sized nanoclusters as both the number of possible atomic configurations and cost per calculation increase rapidly with n. Moreover, for the latter, the oxidation state or charge on each atom is typically chosen and fixed, thus restricting the possible type of bonding in the nanoclusters and therefore reducing the number of minima on the IP landscape.

Ignoring the problem of finding local minima, the success of this approach is dependent on the reliability of the IP, i.e. whether local minima structures found on the IP landscape resemble and have ranks similar to those found on the ES landscape. Assuming there is at least one IP local minimum structure that maps onto each basin on the ES landscape that contains a desired low energy minimum on the ES landscape, then it is simply a matter of refining the stable and metastable IP structures, starting from the IP global minimum and continuing until the ES global minimum is found. But how many IP local minima should be found and then refined? In previous studies[37,43,48,51,55] on nanoclusters of ZnO, TiO_2, ZrO_2, Al_2O_3, and In_2O_3, the local minima on the IP landscape based on the rigid ion model (RM-IP) were found using an evolutionary algorithm that is implemented within the GULP software package[56,57] and then subsequently refined using the shell model (SM-IP, as implemented within GULP) before employing ES methods. In these studies, not only is there better resemblance between SM-IP and ES local minimum structures (than between RM-IP and ES)[37] but also there is a better agreement with the ranking of minima, and in particular, the equivalent IP structure for the ES global minimum nanocluster of size n has a rank nearer to the SM-IP global minimum structure.[48] Thus the expected number of local minima IP structures to refine using ES techniques can be reduced if the SM is employed.

In the approach used to generate the results for $(LaF_3)_n$, we have used the SM during the initial global search rather than as a refinement stage after the search has finished. As the SM is not as robust as the RM, each new configuration is structurally relaxed twice (minimize the energy of formation using standard local optimization techniques): first using loose optimization tolerances and a rigid ion model and then with better tolerances within the shell model. Only energy values obtained when employing the SM are used to assess or compare the quality of candidate clusters and therefore influence the future direction of the global search on the "hybrid" or patchwork of IP landscapes composed of energies from the RM with basin regions replaced with energies from the SM. This work was done using the random and global optimization routines from a newly developed module (Stochastic Cluster Optimization based on Thermodynamical Techniques) of the in-house Knowledge Led Master Code (KLMC) software package.[58]

There are already a number of codes specifically designed for structure prediction,[31,56,59,29,60−66] many of which link into third party electronic structure codes, for example, CASTEP,[67] VASP,[68] CRYSTAL,[69] and NWCHEM,[70] to compute energies and forces and more generally to perform local optimization of structures. KLMC, or more specifically the Knowledge Led Master Code, was created with the desire to: automate many tasks traditionally performed by the user of a range of such third party codes; enable a multistage approach where the KLMC code *learns on the fly* and refines input files that are submitted for new calculations—hence the name *knowledge led*; and be able to exploit massively parallel computer platforms for a more general set of applications that may require statistical sampling. Currently KLMC is capable of updating a simple database of structures (or solutions); performing postanalyses (e.g., computing radial distribution functions, ensemble average—Boltzmann weighted—properties); generating and reading input and outputs files for GULP,[56,57] FHI-AIMS,[71,72] VASP,[68] and NWCHEM;[70] and running these either on the same platform (either through system calls or as library files) or remotely (KLMC runs itself on a local machine and many individual calculations, or tasks on larger resources, elsewhere). Applications include: simple task farming (screening structures from the database through a third-party code); structure prediction of nanosized clusters, surfaces, and bulk phases using a range of global optimization techniques based on basin hopping and genetic algorithms; exploration of ergodic regions (application of the energy lid or threshold algorithm);[73,74] and statistical sampling of solid solutions or multiple point defects in a crystalline solid. In this work, KLMC was used both to

drive random and global optimization routines and to generate and update a structure database; link up with GULP (used to compute and minimize IP energies) during the global optimizations; and link up with the FHI-AIMS code (chosen software package used to compute and minimize ES energies) during the final refinements of structures in the database, and therefore used to automate our approach to predicting the structures of $(LaF_3)_n$ for sizes n = 1 to 6.

2. METHOD

2.1. Energy and Spectroscopic Properties. It is assumed that the configuration adopted by an isolated $(LaF_3)_n$ nanocluster in an experiment is that which minimizes its energy of formation. As in previous work,[48,51,55] four different energy functions are employed, each assumed to be better than the previous one and, importantly, more expensive to compute.

The first energy function is based on the rigid ion model, where each lanthanum cation and fluoride anion is represented as a point charge of $+3e$ and $-1e$, respectively, and the analytical interatomic potential

$$V(r_{ij}) = \frac{q_i q_j}{r_{ij}} + \frac{A_{ij}}{r_{ij}^{12}} + B_{ij}\exp(-r_{ij}/\rho_{ij}) - \frac{C_{ij}}{r_{ij}^{6}} \quad (1)$$

is used to model the interaction between ion i and ion j, which are distance r_{ij} apart. The first term is the Coulomb contribution (in eV) between point charges q_i and q_j, and the remaining terms are a combination of standard Lennard-Jones and Born−Mayer terms. Note the use of subscripts on the potential parameters A, B, C, and ρ as these are species dependent. For the *rigid ion model*, the energy of formation is the sum of all two-body interactions defined by eq 1.

To represent electronic polarization of fluoride ions, the *shell model*[75] is employed (our second energy function). In the shell model, each point charge from the rigid ion model is replaced by two; one represents the nucleus and core electrons and the other, which is connected via a harmonic spring to the first, the center of charge for the valence electrons. With the inclusion of shells, the interatomic potential becomes

$$V(r_{i_c j_c}) = \begin{cases} 0 & i = j \\ \dfrac{q_i q_j}{r_{ij}} & i \neq j \end{cases}$$

$$V(r_{i_c j_s}) = \begin{cases} \dfrac{1}{2}k_{ij}r_{ij}^2 & i = j \\ \dfrac{q_i q_j}{r_{ij}} & i \neq j \end{cases}$$

$$V(r_{i_s j_s}) = \begin{cases} 0 & i = j \\ \dfrac{q_i q_j}{r_{ij}} + B_{ij}\exp(-r_{ij}/\rho_{ij}) - \dfrac{C_{ij}}{r_{ij}^{6}} & i \neq j \end{cases} \quad (2)$$

where the core and shell are indicated by the second level subscripts c and s, respectively; A_{ij} is set to zero (as clusters at this stage would not have very short interatomic distances); and k_{ij} is the spring constant, which is also species dependent. Note that the Born−Mayer and dispersive terms are applied between the shells and that the Coulomb contribution between two point charges of the same ion is not included. Equation 1 is used for cation−cation interactions, eq 2 for anion−anion interactions, and for the cross terms (cation−anion interactions)

$$V(r_{ij_c}) = \frac{q_i q_j}{r_{ij}}$$

$$V(r_{ij_s}) = \frac{q_i q_j}{r_{ij}} + B_{ij}\exp(-r_{ij}/\rho_{ij}) - \frac{C_{ij}}{r_{ij}^{6}} \quad (3)$$

are employed, where i labels cations, j_c the anion cores, and j_s the anion shells. Both the rigid ion and shell models are implemented within the GULP code.[57]

The values for B (in the Born−Mayer term) and C (in the dispersive term) for both the rigid ion model and the shell model are taken from earlier work on lattice and intrinsic defect properties of bulk rare-earth fluorides,[76] where in fact a four-region Buckingham potential between anions was employed. In this variant, only the short-range repulsive Born−Mayer term is applied within the first radial cutoff (C = 0), and only the dispersive van der Waals term is applied outside a greater, third radial cutoff (B = 0). Two polynomials are used between these regions to ensure that this potential is smooth and continuous. For the rigid ion model we have also included the r^{-12} term to penalize interaction distances that are significantly shorter than a typical bond length (A = 1.0 eV Å^{12} for like charged species and 10.0 eV Å^{12} otherwise).

The third and fourth energy functions are based on density functional theory (DFT). Here, we use an all-electron DFT method with a local numerical orbital basis set, as implemented in the FHI-AIMS code (version 051610_1).[71,72] The FHI-AIMS code comes with a number of default basis sets for each atom, with increasing accuracy starting from "tier 1". The tier 2 basis set is reported to provide accuracy between −30.19 to −0.51 meV per La atom and −12.96 to −1.56 meV per F atom. However, due to the strongly ionic nature of these atoms only the tier 1 basis set for La atoms proved necessary when ranking the nanoclusters (these energies will also be used in labeling LM), together with the default "tight" settings for tolerances. When calculating spectroscopic properties an improved basis set is employed; however, when testing the suitability of the SM to rank nanoclusters the tolerances are relaxed to the default "light" settings, and a tier 1 basis set is employed to reduce the computational cost of producing Figure 1 shown in Section 2.2.

To assist in choosing which functional to employ, spectroscopic data are calculated for single atoms employing a range of functionals (see end of Section 2.1). From these results, and as it is also unbiased and is not too computationally expensive, the PBEsol functional[77] is chosen for our third definition, whereas for our fourth definition the hybrid PBEsol0 functional is employed. The hybrid PBEsol0 functional replaces 25% of the PBEsol electron exchange with exact Hartree−Fock like exchange.[77,78] Throughout the paper we will use "RM", "SM", "PBEsol", and "PBEsol0" to indicate which of the four definitions, given above, is employed. Within the DFT approach, the eigenstates obtained from the solution of the Kohn−Sham equations are Gaussian-smeared with a width of 0.0001 eV. While minimizing the PBEsol energy, via structural relaxations of the nanoclusters, scalar-relativistic effects are treated at the scaled zero-order relativistic approximation (ZORA) level,[79] whereas when computing single-point PBEsol and PBEsol0 energies and spectroscopic data the full ZORA level of theory[79] is employed.

dx.doi.org/10.1021/jp406854j | J. Phys. Chem. C 2013, 117, 24003−24014

Table 1. Third Ionization Potential (IP3) for La and Electron Affinity (EA) Values for F

	PBE	PBEsol	PBE0	PBEsol0	G_0W_0/PBEsol0	experiment[84]
IP3 (La), eV	19.85	19.83	19.22	19.32	19.17	19.17
EA (F), eV	3.63	3.66	3.22	3.39	3.13	3.40

To obtain an estimate of the accuracy of calculated ionization potentials (IP) and electron affinities (EA) of the stable clusters, we tested two approaches and four functionals (χ = PBE, PBE0, PBEsol, or PBEsol0) for the component atoms: a single lanthanum and a single fluorine. First, following the ΔSCF approach, we computed the differences in the total self-consistent-field energies (with FHI-AIMS maximum—tier 4—basis set). Later, for the $(LaF_3)_n$ nanoclusters, this equates to

$$\mathrm{IP} = E_{\mathrm{cation}} - E_{\mathrm{neutral}} \tag{4}$$

and

$$\mathrm{EA} = E_{\mathrm{neutral}} - E_{\mathrm{anion}} \tag{5}$$

where E_{cation}, E_{neutral}, and E_{anion} are the total energies for the +1, 0, and −1 charged system, respectively. Returning to the test on individual component atoms, note that total energies for various spin configurations of each atom were investigated, including a doublet for the neutral atoms and a singlet and triplet otherwise. In a second approach that is available in FHI-AIMS, quasiparticle corrections to the χ Kohn−Sham eigenvalues (ε_n^{χ}) are included through the G_0W_0 approximation,[80,81] which combines the single-particle Green's function (G) with the dynamically screened Coulomb interaction (W). The resulting quasiparticle energies (E_n^{QP}) emerge as a first-order perturbation, calculated using χ Kohn−Sham orbitals (ψ_n)

$$E_n^{\mathrm{QP}} \approx \varepsilon_n^{\chi} + \langle \psi_n | G_0W_0(\varepsilon_n^{\chi} - V_{\mathrm{xc}}^{\chi}) | \psi_n \rangle \tag{6}$$

which have a direct correspondence with photoemission (N − 1 electrons) and inverse photoemission (N + 1 electrons) and, in the case of the highest occupied and lowest unoccupied orbital levels of the atom (and later, nanocluster) of interest, measures the respective vertical ionization potentials and electron affinities. This GW approximation has had recent successes in describing both the band structure and defect properties of metal oxide systems.[82,83]

On ionization of LaF_3 nanoclusters one expects that an electron will be removed from a fluoride ion (resulting in a cationic cluster) or an electron added to a lanthanide ion (resulting in an anionic cluster). Therefore, the accuracy of the calculations will be crucially dependent on the reproducibility of the electron affinity of the fluorine atom and the third ionization potential of lanthanum. Comparison of calculated and observed values[84] is provided in Table 1. Note that the calculations confirm the correct ordering of spin states for relevant ions.

The best agreement with experiment is obtained with the G_0W_0/PBEsol0 approach for the ionization potential, whereas the electron affinity is more accurately reproduced using the ΔSCF method also based on PBEsol0. Hence, the PBEsol0 functional has been chosen for computing our final energies of the nanoclusters of interest and the G_0W_0 approach using PBEsol0 (tier 4 basis set) Kohn−Sham orbitals for computing the IP and EA of the lowest-energy PBEsol0 nanoclusters. As these calculations are memory intensive, this approach could only be applied to the smaller nanoclusters. For all sized nanoclusters, the ΔSCF method is employed with the PBEsol functional, which has been used in their geometry optimization. Note that the neutral clusters are assumed to adopt a no spin singlet arrangement, whereas both the anion and cation are assumed to adopt a doublet spin state.

2.2. Generating the Stable and Metastable Configurations. For each cluster size we employ a series of global optimization runs to find the stable and metastable configurations (local minima on the energy landscapes). Each run is based on a sequence of local optimizations using standard relaxation techniques to locate the local energy minimum, and thus the method is referred to as minimum or basin hopping.[24,26,31] In fact two types of basin hopping runs are performed: a standard run that is tuned to find the lower energy minima (including the global minimum) and a continuously randomized run that is tuned in an attempt to find all minima. Of course, finding all minima might be possible for the small clusters, but already for n = 6 there is no guarantee that all minima, including the global minimum, will be found.

Initial, or random, nanoclusters were created by generating random atomic coordinates for the appropriate number of lanthanum and fluorine ions such that all ions are within an (8 Å)^3 or (10 Å)^3 box centered at the origin. A few additional runs were completed with box sizes $L \times L \times 3$ Å and 3 Å × 3 Å × L, with L > 8 Å, to encourage the formation of planar and rod-like clusters.

The atomic coordinates of all new nanoclusters are optimized using the method of conjugate gradients (until the resultant atomic forces are less than 0.05 eV/Å) and the rational function optimizer[85] (to ensure optimization moves away from any saddle point and rapidly converges to the local minimum) to minimize the RM energy. In practice, the atomic coordinates and RM interatomic potentials are fed by the KLMC code into the GULP software (with default optimization tolerances), and then the refined coordinates and RM energy (or error message) are retrieved. For successfully relaxed nanoclusters, each −1|e| point charge is then replaced with two point charges +0.59|e| and −1.59|e| (representing the core and shell of the fluorine anions, respectively), and the coordinates of all point charges are optimized so that the SM energy is minimized. This process is also automated by the KLMC code, which instigates a second call of GULP to use the same two optimization routines but with the SM interatomic parameters and better optimization tolerances (set to 10^{-9}). The optimized atomic coordinates (location of +3|e| and +0.59|e| point charges) and SM energy are retrieved from the GULP output and stored in the KLMC database of candidate structures. Note that a different database library is generated for each system size (composition), which is updated if additional runs are required, and can be programmed to keep the coordinates of only the best and/or worst set of structures or those within a predefined energy range, which might be desirable for larger sized clusters than those studied here.

In an attempt to generate all small nanoclusters and to learn how easy it is to find each individual SM local minimum on this hybrid surface, many random nanoclusters are generated, each optimized following the procedure describe above. This approach is referred to as *random basin hopping* as the new

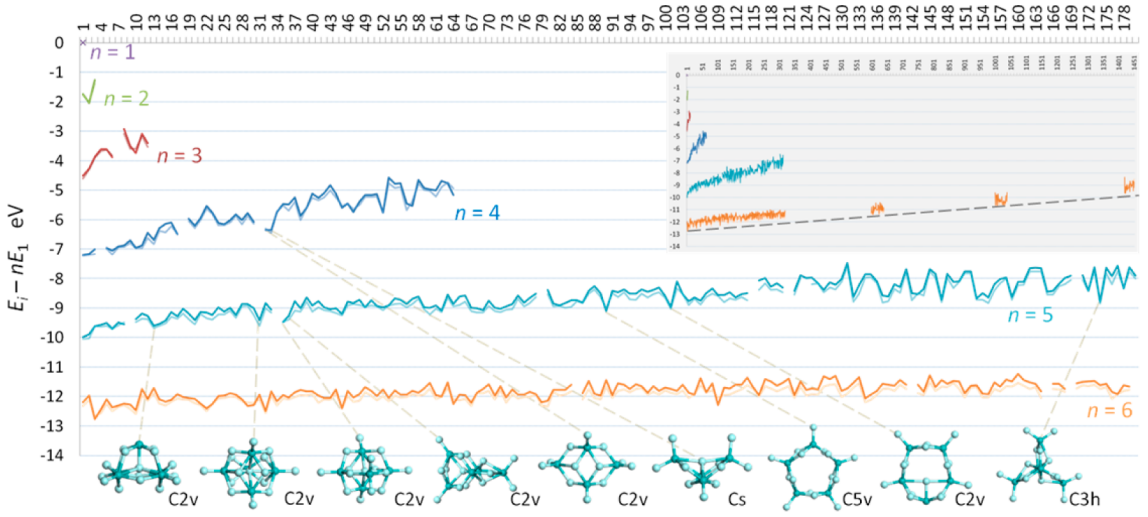

Figure 1. Main panel: Binding energies of $(LaF_3)_n$ clusters as a function of SM rank defined as PBEsol0 (dark lines) and PBEsol (shadow lines) energies, $E_i - nE_1$, for PBEsol optimized structures. Breaks in these lines indicate SM local minima that are unstable on the PBEsol landscape (relaxed to a PBEsol LM already included in the figure). Lower panel: Atomic structure (La and F are shown as darker and lighter balls, respectively) that corresponds to the deep LM in lines for n = 4, 5, and 6. Upper right panel: as with the main panel but for wider range (highest energy SM minima for n = 6 are shown); gaps in n = 6 data correspond to SM minima not refined on the PBEsol landscape; and broken line is a simple guideline.

basin investigated is not influenced by basins already found. The statistics from these gradient quenches from random starting positions are reported below.

For larger clusters this exercise becomes futile, and better tuned global optimization techniques are required; here a Metropolis driven, *basin-hopping* approach is used where a current champion configuration (with the energy of one of the previous basins) does influence the choice of future basins; i.e., the atomic structure of the new trial cluster (before local optimization) will resemble that of this champion. To drive toward the global minimum, or at least toward the bottom of the superbasin, tournaments are simulated where the better (lower-energy) configuration is more likely to become the new champion. In practice, with the first random or seeded cluster defined (after structural relaxation) as the initial champion, a new (or next) trial configuration is created by relaxing the configuration generated by applying small random changes to the configuration of the current champion. The champion is only replaced by the new trial configuration if this trial configuration wins in a pair-wise tournament, where the outcome is determined by the Metropolis criterion.[86] If the simulated temperature parameter used in the Metropolis criterion is set to zero, then the current champion will always be the lowest energy local minimum nanocluster found on that particular run. Random changes, or random steps on the landscape, are applied using one of the following four different phenotype moveclass operators:

(1) Standard Monte Carlo move: each atomic coordinate of the nanocluster is given a random displacement between −S and +S, where S is initially set to 0.8 Å and can increase if the global optimizer is stuck (each new trial nanocluster relaxes back to the current champion).

(2) Randomize solution: the coordinates for a random number of lanthanum cation and fluorine anion pairs are switched.

(3) Twist cluster: a random axis is chosen that passes through the cluster's center of mass. Then all atoms within a random slice along this axis are rotated about this axis by a random angle.

(4) Twin crossover: a copy of the cluster is spliced into itself (crossover moveclass as used in genetic algorithms[25,35]). Essentially, a different random rotation is applied to each identical twin before they are cut into (typically unequal) halves such that when the left-hand of the first is fused to the right-hand of the second the new cluster maintains the correct composition.

These operators are implemented within the newly developed module (Stochastic Cluster Optimization based on Thermodynamical Techniques) of the in-house KLMC software package. After optimizing the new cluster, KLMC checks the interatomic distances and rejects any collapsed or fragmented clusters. In this study, a cluster is deemed collapsed if an interatomic distance less than 2.15 or 2.45 Å between different or like species, respectively, is found and fragmented if all atoms in one fragment are further than 2.75 Å away from all atoms in a different fragment. Note that these chosen collapse (fragmentation) cutoff distances are slightly shorter (longer) than those found in the $(LaF_3)_1$ and $(LaF_3)_2$ SM configurations. Typically 50 000 steps are attempted on each run, and different runs for each size of cluster are continued until KLMC reports that the putative global minimum has been generated at least twice and that, on the last run, there were no new SM minima in the database or significant changes in the probabilities. As a separate stage, using a simple task farming[87] script within KLMC to call FHI-AIMS, configurations within the database are further refined: PBEsol energy is minimized. For each size, the ionization potential and electron affinity are computed for the better PBEsol0 ranked (including the GM) PBEsol optimized nanoclusters.

It is assumed that, using the set of stable and metastable SM configurations as initial atomic coordinates and a standard local optimization routine, the lowest energy PBEsol or PBEsol0 configuration can be obtained for each value of n. Ideally, the lowest energy SM and PBEsol (or PBEsol0) configurations are the same (or at least refinement of the former readily produces

dx.doi.org/10.1021/jp406854j | J. Phys. Chem. C 2013, 117, 24003−24014

the latter). However, in practice, the ranking on different energy landscapes is unlikely to be the same, so how many configurations in the database of SM minima configurations should be refined? For the smaller sized nanoclusters there are not many candidates in the database to refine, and refinement is relatively cheap. In Figure 1 we plot the minimized PBEsol and PBEsol0 energies as a function of the rank of the nanocluster as originally found using the SM. For $n < 6$ we were able to do this for all nanoclusters found; i.e., all configurations for a particular size were entered into the KLMC database. The PBEsol data shadow the PBEsol0 data (lines in Figure 1 typically mirror each other), and generally both increase with SM rank. This appears to hold for $n = 6$ where a straight line has been added through the PBEsol energies for SM ranked 1 to 320, 600 to 640, 1000 to 1040, and above 1420. Thus, we can safely assume that we only need to refine the better ranked configurations; moreover, the global PBEsol minimum for each size is found within the top six SM local minima. Note that occasionally two or more SM configurations refine to the same PBEsol configuration. In such cases one of these clusters typically requires many more refinement steps as they collapse into the basin containing the other SM energy configuration; data for such clusters have been removed from Figure 1 and appear as breaks in the lines.

The local maxima and local minima in Figure 1 correspond to atomic configurations that were SM ranked better and worse, respectively, than those found on the PBEsol landscape. Atomic configurations for deep local minima along the $n = 4$, 5, and 6 lines are also shown in Figure 1. Most of the other local minima have no symmetry; thus, it appears that the SM employed in this work penalizes, too heavily, clusters of higher symmetry—possibly a result of omitting shells on the lanthanum ions.

3. RESULTS

For convenience, the nanoclusters are labeled according to their size and (alphabetical) rank as found by SM, PBEsol, and PBEsol0; e.g., 6aba indicates that the $(LaF_3)_6$ nanocluster is ranked as the global minimum (label "a") for both SM and PBEsol0 but only the second lowest PBEsol configuration.

Configurations for the smallest LaF_3 nanoclusters are shown in Figure 2. Only one configuration, a trigonal planar structure with three La−F bond lengths of 2.265 Å, was found on the SM landscape for the smallest size, $(LaF_3)_1$. After further refinement (minimization of PBEsol) the bond lengths shorten to 2.09 Å, and the central La moves 0.53 Å out of the plane of fluorine atoms resulting in a change of point symmetry from D_{3h} to C_{3v} and a reduction in the F1−La3−F1 bond angle from 120° to 113.5°. Note the use of numbers in the labeling of atoms to indicate their coordination. For the smallest size cluster, where atoms are most severely undercoordinated as compared to that observed in the bulk phase, it is not uncommon that the global minimum IP configuration is actually a saddle point on the PBEsol energy landscape.[48] Recent spin−orbit coupled DFT calculations also yield a C_{3v} configuration (F1−La3−F1 bond angle of 113.3°) as a minimum and the flat D_{3h} structure as a saddle point,[88] confirming further the early coupled cluster calculations[89] that give a bond angle of 109.0°.

The ionization potential and electron affinity of the nanocluster 1aaa is calculated (PBEsol0 tier 4 G_0W_0) to be 12.34 and 0.21 eV, which compares well with 12.32 and 0.23 eV that were obtained using PBE0. Using the ΔSCF PBEsol approach (eqs 4 and 5), slightly lower values of the ionization

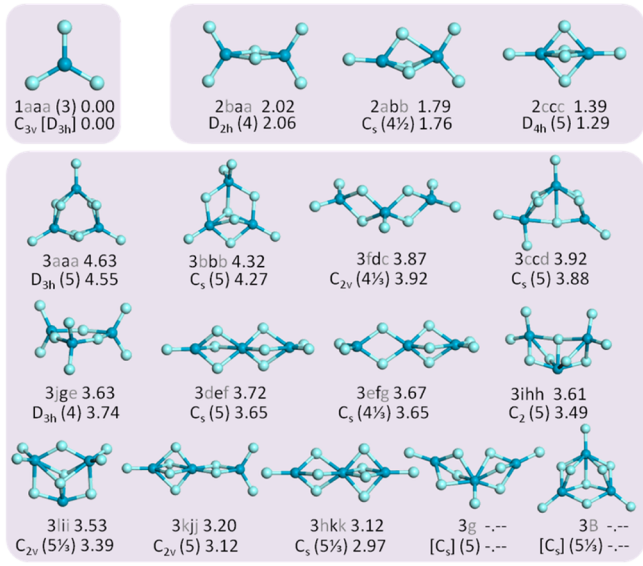

Figure 2. PBEsol [and, for the last two configurations, SM] optimized atomic structure of $(LaF_3)_1$, $(LaF_3)_2$, and $(LaF_3)_3$ nanoclusters: dark (light) spheres represent lanthanum (fluorine) atoms; PBEsol (upper) and PBEsol0 (lower) total energies relative to n isolated $(LaF_3)_1$ nanoclusters are in eV to two decimal places; average coordination number of lanthanum is given in parentheses; the lower label indicates the point symmetry of the cluster, whereas the upper label indicates the number of LaF_3 units, the SM rank (gray font), PBEsol rank, and PBEsol0 rank (gray font) using the convention that "a" is the global minimum.

potential and electron affinity are calculated: 11.51 and 0.18 eV. Again, using different functionals gives similar values (see Table 2). Note that the electron affinity is more sensitive than the ionization potential to the choice of tier level, which increases with the number of basis functions employed in both approaches, and thus calculated values provide predicted lower bounds for the electron affinity of the nanoclusters.

Three configurations for $(LaF_3)_2$ nanoclusters were found, although in principle one can construct six configurations with differing numbers of bridging fluorine atoms between the two lanthanum atoms, and a further six if the F1 atoms are less evenly distributed on the two lanthanum atoms. Using the KLMC random search approach (random basin hopping), there was found to be a 23.5% chance of generating the lowest SM energy cluster, 2abb, 76.4% for 2baa, and just over 0.1% for 2ccc. After final refinements, the ranking of the lowest two configurations switches; thus, fortuitously, the lowest PBEsol energy nanocluster resides in the largest SM energy basin and therefore is easiest to find. The PBEsol0 (SM) energy differences between these lowest two configurations is 0.3 eV (0.1 eV), whereas there is a bigger gap between the highest two configurations, 0.5 eV (0.5 eV). Unlike the average coordination number (or number of bonds shown as sticks in Figure 2), which increases with the number of bridging fluorine atoms, the PBEsol0 energy, or stability, decreases; the large lanthanum cation prefers to have a regular distribution of nearest fluorine anions. Configuration 2baa, which is composed of two edge-sharing LaF_4 tetrahedra with bond angles F1−La4−F1 of 116.6°, F1−La4−F2 of 115.3°, and F2−La4−F2 of 71.2°, has the lowest PBEsol0 (and PBEsol) energy. The four La−F1 bonds in this configuration are also (cf. configuration 1aaa) 2.09 Å, whereas the four La−F2 interatomic distances are increased, due to the repulsion between the like charged ions,

dx.doi.org/10.1021/jp406854j | J. Phys. Chem. C 2013, 117, 24003−24014

Table 2. First Ionization Potential (IP) and Electron Affinity (EA) Values for PBEsol Optimized $(LaF_3)_1$

	PBE	PBEsol	PBE0	PBEsol0	G_0W_0/PBE0	G_0W_0/PBEsol0
IP, eV	11.50	11.51	12.19	12.35	12.32	12.34
EA, eV	0.20	0.18	0.23	0.35	0.23	0.21

to 2.34 Å. All three $(LaF_3)_2$ nanoclusters have a similar PBEsol La−F2 average bond length (2.34, 2.37, and 2.36 Å for 2baa, 2abb, and 2ccc, respectively), whereas the La−La interatomic distance decreases with the number of bridging fluorine atoms (3.80, 3.48, and 3.06 Å). In passing we note that the original predicted SM configurations have similar interatomic distances and bond angles. For example, the La−La separation also decreases with the number of bridging fluorine atoms (3.85, 3.52, and 3.17 Å), and 1baa has F1−La4−F2 of 111.6° and a reduced F2−La4−F2 angle of 73.2° and elongated La4−F2 bond length of 2.40 Å (cf. 2.27 Å for La4−F1). The ionization potential and electron affinity are calculated (PBEsol0 tier 4 G_0W_0) to be 12.51 and 0.76 eV for nanocluster 2baa and 12.13 and 1.59 eV for 2abb. Using the ΔSCF PBEsol approach (eqs 4 and 5), slightly lower values of the ionization potential and electron affinity are again obtained: 10.84 and 0.23 eV for 2baa and 10.70 and 0.23 eV for 2abb. For completeness, 10.75 and −0.14 eV are calculated for the ionization potential and electron affinity, respectively, of nanocluster 2ccc.

Eleven PBEsol energy minima were found for $(LaF_3)_3$ nanoclusters. Using random basin hopping, the probability of finding one of the best three nanoclusters was extremely high: 18.6% for 3aaa, 36.3% for 3bbb, and 29.5% for 3fdc. The expectation of finding a different configuration is just 15.6%, which includes the lowest energy 1D rod configurations (3def at 3.8% and 3efg at 5.1%) and at 6.1% the corner-sharing tetrahedra that form the 3jge ring configuration, with D_{3h} point symmetry (all others each have a probability of less than 0.004). As found for other compounds,[37] there are more energy minima on the RM landscape than the SM. In this case, the configuration labeled 3B in Figure 2 has the second lowest RM energy but relaxes to 3aaa on both the SM and the PBEsol energy landscape—already emphasizing the better match between SM and PBEsol. There is also a very good agreement in ranking obtained from SM and PBEsol0; the only notable exception in the lowest-energy $(LaF_3)_3$ clusters shown in Figure 2 is the ring of corner-sharing tetrahedra, 3jge, which is ranked 10 (SM) and 5 (PBEsol0). Note that SM configuration 3g relaxes to 3fdc.

It is useful to see whether a structural pattern can be repeated to form a series of larger clusters. For each value of $n > 2$ there is a ring configuration of lanthanum atoms with each pair bridged by two fluorine atoms; likewise, there is a ring configuration of lanthanum atoms with each pair bridged by one fluorine atom. Using a polyhedral description, as opposed to the ball-and-stick figures, the members of the first series consist of edge sharing LaF_5 square-based pyramids, whereas members of the second series consist of corner-sharing LaF_4 tetrahedra. 3aaa is the smallest member for the edge-sharing series and 3jge for the corner-sharing series. Members of both series have the same point symmetry, D_{nh}, where n is the size of the $(LaF_3)_n$ nanocluster. During the search on landscapes for $n > 3$, larger members should be found for both series, although one can expect larger members to be metastable and that their rank increases (diminishes) with n.

Similarly, it is useful to know whether larger particles are constructable from smaller nanoclusters already found. All three $(LaF_3)_2$ local minima configurations can be used as bricks to construct a number of different rod nanoclusters composed of collinear lanthanum atoms. Configuration 3def is essentially two merged units of 2abb; 3efg is 2abb and 2baa; 3fdc is two units of 2baa (lanthanum atoms form a curved line, which if closed forms configuration 3aaa); 3hkk is 2abb and 2ccc; and 3kjj is 2baa and 2ccc. Rods, which terminate with a lanthanum rather than at least one fluorine atom (for example, two units of 2ccc merged to create a configuration composed of eight bridging fluorine atoms), are unstable. Larger nanorods, containing any combination of $n = 2$ nanoclusters, provided the number of 2ccc bricks is no greater than one more than the number of 2baa, are found, but with a small probability during the random gradient quench runs, provided the initial shape of the starting box is cubic, particularly for larger values of n. As found for the larger ring nanoclusters, the rank of these rods is progressively worse as the size, or length, increases.

As n increases, so does the coordination of lanthanum atoms for the PBEsol0 global minimum structures: 3, 4, and 5 for 1aaa, 2baa, and 3aaa, respectively. As found for $n = 2$, the lowest energy $n = 3$ nanocluster, 3aaa, does not have the largest number of bonds. The ionization potential for 3aaa is calculated (PBEsol0 tier 3 G_0W_0) to be 12.47 eV, whereas the electron affinity is 0.75 eV. Using the ΔSCF (PBEsol tier 4) approach, slightly lower values are obtained: 10.61 and 0.28 eV. The ionization potential for the PBEsol metastable configurations 3fdc and 3jge is calculated to be 10.48 and 10.50 eV, respectively, and 0.52 and 0.66 eV for their respective electron affinity. Thus, by breaking one of the three La−F−La bridging pairs and opening up the three-ring or breaking one bridge in every pair and keeping a three-ring configuration, the ionization potential is lowered, whereas the electron affinity (and lanthanum average coordination) is increased (decreased).

Sixty-four SM energy minima were found for $(LaF_3)_4$ nanoclusters, and of these sixty-one are PBEsol energy minima. Using random basin hopping, 4eef at 15.2% was the easiest configuration found; then 4yt- at 13.9% and 4bcb at 12.3%—all others have a probability of less than 7%. Nanocluster 4eef is ranked fifth for both SM and PBEsol and sixth for PBEsol0 and is essentially a ring of four edge-sharing square based pyramids (configuration 4jfd) but with one fluorine atom at the center from one of the four two rings (after rotation) (see Figure 3). Nanocluster 4yt- (ranked 25th for SM and 21st for PBEsol—note that the higher quality PBEsol0 was not performed for all LM, although from Figure 1 it is reasonable to assume 4yt- is ranked ∼21st for PBEsol0) is composed of a three-ring capped on both sides (like nanocluster 3lii) and a two-ring (nanocluster 2baa) that is perpendicular to the three-ring. Nanocluster 4bcb (ranked second for SM and PBEsol0, third for PBEsol), with C_{3v} point symmetry, is composed of two layers: a three ring that is also capped on both sides and a LaF_4 tetrahedron.

Configuration 4aba, with C_{2v} point symmetry, is the lowest SM and PBEsol0 energy $(LaF_3)_4$ nanocluster (and ranked second for PBEsol) and is composed of one central fluorine atom, two five-coordinated and two six-coordinated lanthanum atoms, and seven bridging and four singly coordinated fluorine

dx.doi.org/10.1021/jp406854j | J. Phys. Chem. C 2013, 117, 24003−24014

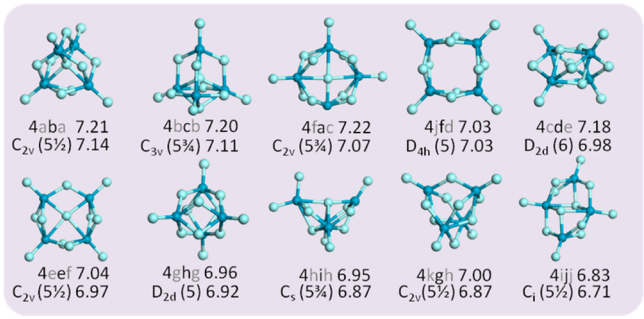

Figure 3. PBEsol optimized atomic structures for $(LaF_3)_4$ nanoclusters, where dark (light) spheres represent lanthanum (fluorine) atoms. For explanation of labels see caption for Figure 2

atoms. The probability of finding this global minimum using a random search was 4.5%. The ionization potential and the electron affinity calculated (ΔSCF PBEsol tier 3) for the better ranked $(LaF_3)_4$ nanoclusters are 10.52 and 0.36 eV for 4aba, 10.54 and 0.30 eV for 4bcb, 10.37 and 0.58 eV for 4fac, 10.48 and 0.73 eV for 4jfd (the four ring of edge-sharing square based pyramids), and 10.60 and 0.29 eV for 4cde. As already observed for $(LaF_3)_3$, the value of the electron affinity typically decreases with an increase in the average coordination number of the lanthanum ions. The exception to this trend is found for configuration 4fac, which has a greater electron affinity and an exposed lanthanum ion (convex environment—lanthanum ion not coplanar with the outer four anions but slightly displaced away from the center of the nanocluster with F−La−F internal bond angles of 148° rather than 180°).

The ring composed of four corner-sharing tetrahedra lies at the opposite end of the ranking scale; ranked 64th, or last, for SM and 51st for PBEsol. The chain of four edge-sharing tetrahedra (lanthanum atoms not collinear but oscillate) is PBEsol ranked 35th, whereas a flower of three two-rings (three 2baa clusters with a common central lanthanum atom arranged with D_3 point symmetry) is PBEsol ranked 38th. The rod-like structures, described earlier, are also poorly ranked; for example, a chain of three 2abb Lego-units is PBEsol ranked 36th, of two 2abb and one 2baa is PBEsol ranked 39th, 48th, and 49th, of two 2baa and one 2ccc is PBEsol ranked 52nd, and of two 2abb and one 2ccc is PBEsol ranked 53rd and 60th (depending on order of bricks). The highest PBEsol energy local minimum $(LaF_3)_4$ nanocluster is composed of a three-ring (cf. 3jge) with one lanthanum atom connected to the fourth (five coordinated) lanthanum atom via four bridging fluorine atoms (cf. 2ccc).

Results for $(LaF_3)_5$ nanoclusters are presented in Figure 4. A perfect match is found in the SM, PBEsol, and PBEsol0 ranking of the top two nanoclusters. Both these configurations have one highly coordinated fluorine ion surrounded by all five cations forming a square-based pyramid (sbp). Each cation has a singly coordinated fluorine ion, which sits at one of the vertices of a larger sbp, and the capping cation for both configurations has a coordination of seven. The cations forming the base of the inner sbp are bridged by either one or a pair of anions, two pairs for the GM, and three for 5bbb—thus the atoms of the GM configuration have a lower average coordination. An ionization potential of 10.52 eV and an electron affinity of 0.49 eV were calculated (ΔSCF PBEsol (tier 3)) for 5aaa.

The GM is in fact the easiest LM to find; the probability of generating 5aaa using the random basin approach is 0.106 (just

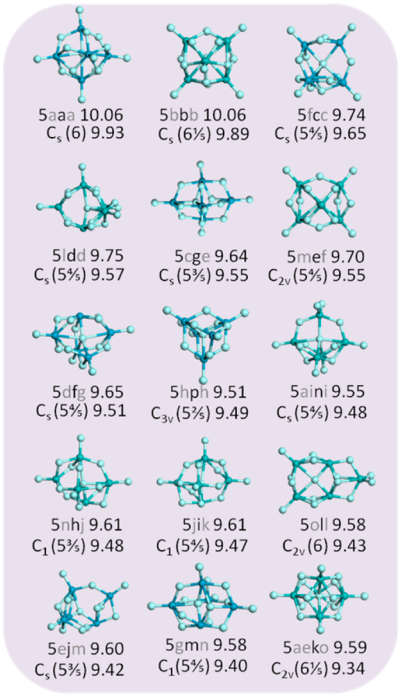

Figure 4. PBEsol minimized atomic structures for $(LaF_3)_5$ nanoclusters, where dark (light) spheres represent lanthanum (fluorine) atoms. For explanation of labels see caption for Figure 2

over 10%), whereas for 5bbb it is just 0.003. The second easiest $n = 5$ nanocluster to find, with a probability of 0.089, is 5ae-k-o, which is SM ranked 30th, PBEsol ranked 11th, has one of the highest symmetries (C_{2v}), and is composed of ions with one of the highest average coordinations (6(1/5)). The third easiest $(LaF_3)_5$ nanocluster to find is that of 5fcc, with a probability of 0.036. The probability of generating the other lower SM energy LMs, 5cge, 5dfg, and 5ejm, is 0.012, 0.002, and 0.015, respectively. Configuration 5hph is the highest symmetry $(LaF_3)_5$ nanocluster shown in Figure 4 and, in a similar way 4bcb was described earlier, can be constructed of three layers: LaF_4 tetrahedron, a middle layer composed of a central F anion in a La_3F_3 ring that is surrounded by a further three F anions and a further LaF_4 tetrahedron (but note that the central F anion is displaced toward one of the tetrahedra).

The GMs for $(LaF_3)_6$ nanoclusters, shown in Figure 5, are predicted to have high symmetry: 6caa has C_{4v} symmetry, whereas for the SM GM, 6ano, it is D_{2h}. Curiously, both configurations have exposed cations: 6ano has two cations which are bonded to six anions contained in one hemisphere, and 6caa has one exposed cation that is bonded to five anions. Moreover, the exposed cations in 6ano are in a concave environment (not coplanar with the outer four anions but slightly displaced toward the center of the nanocluster with F2−La6−F2 external bond angles of 176°, rather than 180°), whereas the 6caa cation is in a more exposed convex environment (F2−La5−F2 internal bond angles of 159.3°). There are other similar examples, like 6hqk, but given the larger number of anions (1:3) one might expect the large cations to be surrounded by anions. In the $(LaF_3)_6$ nanocluster that was found to have the highest symmetry, 6as-g-f, there are only four unique atomic sites: six octahedral cationic sites and six anionic sites that form two La_3F_3 rings that are parallel to each other and exactly out of phase, and six singly coordinated anionic sites that are outside and six anionic sites that are between these

dx.doi.org/10.1021/jp406854j | J. Phys. Chem. C 2013, 117, 24003−24014

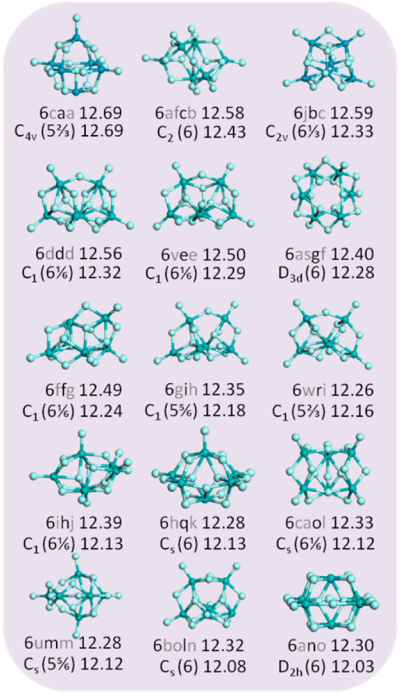

Figure 5. PBEsol minimized atomic structures for $(LaF_3)_6$ nanoclusters, where dark (light) spheres represent lanthanum (fluorine) atoms. For explanation of labels see caption for Figure 2

two rings. An ionization potential (IP) of 10.19 and an electron affinity (EA) of 0.86 eV were calculated (ΔSCF PBEsol tier 3) for 6caaa. The higher EA could be related to the exposed cation, and in fact 6as-g-f, which does not have exposed cations, has a lower value of 0.54 eV (IP = 10.39 eV). However, 6ano, which also has an exposed cation, has an EA value of 0.51 eV (IP = 10.22 eV), perhaps indicating the importance of the direction the bond angle points.

Values of the ionization potential and electron affinities for all the $(LaF_3)_n$ global minima are plotted in Figure 6. Although a trend in these values, with respect to the nanocluster size, can be seen, changes are modest. For comparison, the experimental conduction and valence bands, extracted from ref 90 for bulk

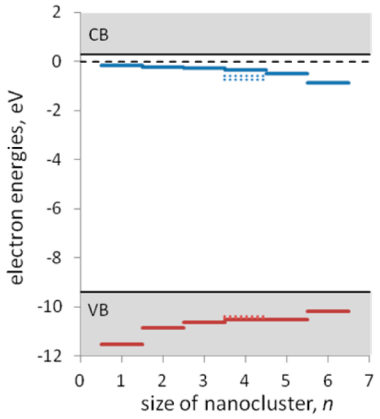

Figure 6. Calculated vertical ionization energies (red) and electron affinities (blue) of the $(LaF_3)_n$ global minima (solid lines) and two local minima (dotted lines), 4fac and 4ffd, relative to the vacuum (broken line) and experimental valence and conduction bands (VB and CB shaded regions) for the bulk phase.[90]

LaF_3, are also shown. However, greater band gap values have also been reported in the literature (see refs 91 and 92, for example, which report a gap of 10.1 and 10.3 eV, respectively). Assuming that the increase in the gap value is entirely due to downshift of the valence band, the valence band edge has the value of −9.6 eV, just above that of the largest nanocluster. However, the exact position of the edges and the value of the gap would be heavily affected by the disorder in the fluoride sublattice due to exceptionally low barriers for fluorine vacancy diffusion.[93] As reported earlier, the nanocluster electron affinity is dependent on the average coordination of lanthanum and whether there is an exposed cation. The changes are again modest (see dotted lines in Figure 6) and is of the same magnitude as the difference found between n = 5 and 6, the latter of which has an exposed cation.

The average coordination of $(LaF_3)_n$ GM, unsurprisingly, increases with n (see Figure 7), where the actual coordination

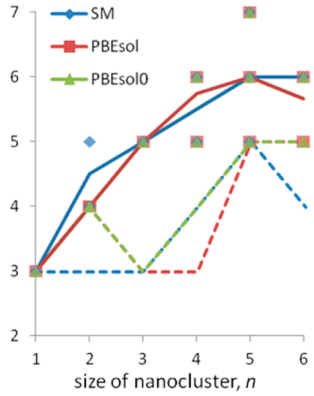

Figure 7. Actual (symbols) and average (solid lines) coordination numbers of La and the number of singly coordinated F (broken lines) in GM configurations of $(LaF_3)_n$.

numbers are also presented. Due to the higher magnitude of the charge on the cations, the La cations typically sit within the nanoclusters (i.e., outer ions tend to be F anions). However, given the coordination of La in the bulk phase is 11, one can expect the size of the GM nanocluster to be much larger than that found for n = 6 before "bulk-like" cuts are predicted. In contrast, higher coordination numbers for fluorine anions have already been found than that adopted in bulk; the coordination number of bulk F^- is either three or four, whereas both 5aaa and 6caa have one fluorine ion that has a coordination number of five. Although the number (fraction) of singly coordinated fluorine anions gradually increases (rapidly decreases) with n, beyond n = 2 it is not greater than the number of outer cations.

4. DISCUSSION

The stable and metastable PBEsol configurations of $(LaF_3)_n$ nanoclusters have been predicted for n = 1−6. Used for data-mining,[94] these can also help in the search for initial atomic structures for other 1−3 compounds for the same values of n. The approach successfully developed and used here was to first find approximate atomic configurations on the energy landscape that is much cheaper to evaluate; the parameters of the shell model were refined elsewhere[76] to reproduce the structure of bulk LaF_3. Standard local optimization methods[57] were employed to relax trial (random) atomic configurations, whereby the polarization of the ions is initially constrained to improve convergence to local energy minima. It was shown

dx.doi.org/10.1021/jp406854j | J. Phys. Chem. C 2013, 117, 24003−24014

that, for each value of n, there is a good match between the ranking of local minima based on shell model energies and that based on DFT (using the PBEsol functional or the PBEsol0 hybrid functional). In fact the match is sufficient that if the better ranked PBEsol energy minima is sought then most of the shell model minima can be safely ignored (only the better ranked shell model minima need to be refined using the more computationally expensive electronic structure approach). This approach is expected to be successfully applied to larger sized clusters (without any further need to find all local minima) and is currently being performed using the in-house KLMC software, which contains the global optimization algorithms and modules for updating a database as well as automating calls to atomic structure and electronic structure software (GULP[57] and FHI-AIMS[71,72]).

The smallest stoichiometric (singlet spin state) LaF_3 GM nanocluster has C_{3v} symmetry, as opposed to the planar D_{3h} configuration that was found during the initial search on the energy landscape defined by interatomic potentials. In fact, further PBEsol calculations revealed a triplet metastable C_{2v} configuration. For the three $n = 2$ nanoclusters, the lanthanum ions are bridged by either two, three, or four fluorine anions, with remaining fluorine anions only singly coordinated. Comparing these three configurations, the predicted PBEsol (and PBEsol0) rank improves by reducing the number of bridges and, therefore, the total number of La−F bonds. For larger-sized low-energy nanoclusters, bridge pairs or trios are also found, and again, bridges formed of even more fluorine anions are heavily penalized in energy or nanocluster ranking. Furthermore, symmetrical configurations were found to be typically more stable, a trend similar to that found for nanoclusters of 1−1 compounds[37] but unlike 2−3 compounds.[55] As expected, the outer ions of the low energy nanoclusters are composed of fluorine anions, since the lanthanum cations have a greater charge. As the size of the nanocluster increases, fluorine anions are also found within; in some cases, they adopt a higher coordination than that found in the bulk. The average coordination of lanthanum in the GM structures increases from three, for $n = 1$, to six, for $n = 5$ and 6, and is much smaller than that seen in the bulk phase (where the coordination number is eleven). In fact, it is not yet clear what value of n is required before a coordination number of eleven will be seen in the GM nanocluster configurations. To summarize, the atomic structure of the nanoclusters can be seen to evolve with size from a trigonal pyramid to ring structures and, finally, to compact symmetrical configurations as the coordination of higher charged La gradually increases. There is also a trend for the external surface of LaF_3 nanoclusters to be decorated by singly coordinated fluorine anions, one per outer La ion for larger nanoclusters. Finally, values of the ionization potential and electron affinities were calculated in the hope that these may prove useful for comparison with future experimental measurements. Typically, a higher electron affinity was found for nanoclusters with exposed cations that also sit further out than neighboring outer anions. Moreover, while the calculated value for the ionization potential (IP) decreased, the electron affinity (EA) for the GM $(LaF_3)_n$ nanoclusters increased with n; from the ΔSCF (PBEsol) approach, IP = 11.51, 10.84, 10.61, 10.52, 10.52, and 10.19 eV and EA = 0.18, 0.23, 0.28, 0.36, 0.49, and 0.86 eV. For fixed n, a greater electron affinity was also typically found for nanoclusters with a lower average coordination number, provided there were no exposed cations.

AUTHOR INFORMATION

Corresponding Author

*E-mail: scott.woodley@ucl.ac.uk.

Notes

The authors declare no competing financial interest.

ACKNOWLEDGMENTS

SMW acknowledges Volker Blum, Alexey A. Sokol and Andrew J. Logsdail for useful discussions, Yee Chow for developing the SCOTT routines in KLMC, and EPSRC (EP/F067496 and EP/I03014X) for computer resources and financial support.

REFERENCES

(1) Gregson, D.; et al. The structure of LaF_3 - a single-crystal neutron-diffraction study at room-temperature. *Acta Crystallogr., Sect. B: Struct. Commun.* **1983**, *39*, 687−691.

(2) Lyon, W. G.; et al. Thermodynamics of lanthanide trifluorides. 1. Heat-capacity of lanthanum trifluoride, LaF_3 from 5 to 350-degrees-K and enthalpies from 298-degrees-KA to 1477-degrees-K. *J. Chem. Phys.* **1978**, *69*, 167−173.

(3) azom.com. *Lanthanum fluoride (LaF_3) - properties and applications*, http://www.azom.com/article.aspx?ArticleID=2348 (accessed 2004).

(4) Popov, P. A.; et al. Thermal conductivity of LaF_3-based single crystals and ceramics. *Inorg. Mater.* **2012**, *48*, 304−308.

(5) Mazzolai, G.; Mazzolai, F. M.; Toncelli, A.; Tonelli, M. *Ultrasonic propagation in, and elastic constants of, BaY_2F_8 single crystals*; Scitech Publications Ltd.: India, 2002; Vol. *206*−*2*.

(6) Dubinskii, M. A.; Semashko, V. V.; Naumov, A. K.; Abdulsabirov, R. Y.; Korableva, S. L. Spectroscopy of a new active medium of a solid-state UV laser with broadband single-pass gain. *Laser Phys.* **1993**, *3*, 216−217.

(7) Janssens, S.; Williams, G. V. M.; Clarke, D. Systematic study of sensitized LaF_3:Eu^{3+} nanoparticles. *J. Appl. Phys.* **2011**, DOI: 02350610.1063/1.3531994.

(8) Lorbeer, C.; Mudring, A.-V. White-light-emitting single phosphors via triply doped LaF_3 nanoparticles. *J. Phys. Chem. C* **2013**, *117*, 12229−12238.

(9) Cho, W. I.; Yi, C. W.; Ju, J. B.; Cho, B. W.; Yun, K. S. Characteristics of a thin-film LaF_3 solid electrolyte for oxygen sensing. *Sens. Actuator B: Chem.* **1991**, *5*, 149−153.

(10) Catlow, C. R. A.; et al. Modelling nano-clusters and nucleation. *Phys. Chem. Chem. Phys.* **2010**, *12*, 786−811.

(11) Catlow, C. R. A.; et al. Advances in computational studies of energy materials. *Philos. Trans. R. Soc. A: Math. Phys. Eng. Sci.* **2010**, *368*, 3379−3456.

(12) Catlow, C. R. A.; Hamad, S.; DiTommaso, D.; Sokol, A. A.; Woodley, S. M. In *Turning points in solid-state, materials and surface science*; Harris, K. D. M., Edwards, P. P., Eds.; The Royal Society of Chemistry: London, 2008; Ch. 11, pp 180−207 .

(13) Catlow, C. R. A.; French, S. A.; Sokol, A. A.; Al-Sunaidi, A. A.; Woodley, S. M. Zinc oxide: a case study in contemporary computational solid state chemistry. *J. Comput. Chem.* **2008**, *29*, 2234−2249.

(14) Twu, Y. J.; Conover, C. W. S.; Yang, Y. A.; Bloomfield, L. A. Alkali-halide cluster ions produced by laser vaporization of solids. *Phys. Rev. B* **1990**, *42*, 5306−5316.

(15) Doye, J. P. K.; Wales, D. J. Structural transitions and global minima of sodium chloride clusters. *Phys. Rev. B* **1999**, *59*, 2292−2300.

(16) Campana, J. E.; et al. Effect of cluster surface energies on secondary-ion-intensity distributions from ionic-crystals. *Phys. Rev. Lett.* **1981**, *47*, 1046−1049.

(17) Shevlin, S. A.; et al. Structure, optical properties and defects in nitride (III-V) nanoscale cage clusters. *Phys. Chem. Chem. Phys.* **2008**, *10*, 1944−1959.

(18) Sanville, E.; Burnin, A.; BelBruno, J. J. Experimental and computational study of small (n=1−16) stoichiometric zinc and

cadmium chalcogenide clusters. *J. Phys. Chem. A* **2006**, *110*, 2378−2386.
(19) Burnin, A.; BelBruno, J. J. $Zn_nS_m^+$ cluster production by laser ablation. *Chem. Phys. Lett.* **2002**, *362*, 341−348.
(20) Woodley, S. M.; Sokol, A. A.; Catlow, C. R. A. Structure prediction of inorganic nanoparticles with predefined architecture using a genetic algorithm. *Z. Anorg. Allg. Chem.* **2004**, *630*, 2343−2353.
(21) Kasuya, A.; et al. Ultra-stable nanoparticles of CdSe revealed from mass spectrometry. *Nat. Mater.* **2004**, *3*, 99−102.
(22) Hartke, B. Global optimization. *Wiley Interdiscip. Rev.-Comput. Mol. Sci.* **2011**, *1*, 879−887, DOI: 10.1002/wcms.70.
(23) Woodley, S. M.; Catlow, R. Crystal structure prediction from first principles. *Nat. Mater.* **2008**, *7*, 937−946.
(24) Cheng, L. J.; Feng, Y.; Yang, J.; Yang, J. L. Funnel hopping: searching the cluster potential energy surface over the funnels. *J. Chem. Phys.* **2009**, DOI: 21411210.1063/1.3152121.
(25) Deaven, D. M.; Ho, K. M. Molecular-geometry optimization with a genetic algorithm. *Phys. Rev. Lett.* **1995**, *75*, 288−291.
(26) Goedecker, S. Minima hopping: an efficient search method for the global minimum of the potential energy surface of complex molecular systems. *J. Chem. Phys.* **2004**, *120*, 9911−9917.
(27) Doll, K.; Schön, J. C.; Jansen, M. Ab initio energy landscape of LiF clusters. *J. Chem. Phys.* **2010**, DOI: 02410710.1063/1.3455708.
(28) Hartke, B. Global geometry optimization of clusters using genetic algorithms. *J. Phys. Chem.* **1993**, *97*, 9973−9976.
(29) Johnston, R. L. Evolving better nanoparticles: genetic algorithms for optimizing cluster geometries. *Dalton Trans.* **2003**, 4193−4207.
(30) Wang, Y.; Zhuang, J.; Ning, X. J. Global optimization method for cluster structures. *Phys. Rev. E* **2008**, DOI: 02670810.1103/PhysRevE.78.026708.
(31) Wales, D. J.; Doye, J. P. K. Global optimization by basin-hopping and the lowest energy structures of Lennard-Jones clusters containing up to 110 atoms. *J. Phys. Chem. A* **1997**, *101*, 5111−5116.
(32) Flikkema, E.; Bromley, S. T. Dedicated global optimization search for ground state silica nanoclusters: $(SiO_2)_N$ (N=6−12). *J. Phys. Chem. B* **2004**, *108*, 9638−9645.
(33) Wootton, A.; Harrowell, P. Inorganic nanotubes stabilized by ion size asymmetry: energy calculations for AgI clusters. *J. Phys. Chem. B* **2004**, *108*, 8412−8418.
(34) Wang, J. G.; Ma, L.; Zhao, J. J.; Jackson, K. A. Structural growth behavior and polarizability of Cd_nTe_n (n=1−14) clusters. *J. Chem. Phys.* **2009**, DOI: 21430710.1063/1.3147519.
(35) Roberts, C.; Johnston, R. L. Investigation of the structures of MgO clusters using a genetic algorithm. *Phys. Chem. Chem. Phys.* **2001**, *3*, 5024−5034.
(36) Haertelt, M.; et al. Structure determination of neutral MgO clusters-hexagonal nanotubes and cages. *Phys. Chem. Chem. Phys.* **2012**, *14*, 2849−2856.
(37) Al-Sunaidi, A. A.; Sokol, A. A.; Catlow, C. R. A.; Woodley, S. M. Structures of zinc oxide nanoclusters: as found by evolutionary algorithm techniques. *J. Phys. Chem. C* **2008**, *112*, 18860−18875.
(38) Wang, B.; Nagase, S.; Zhao, J.; Wang, G. Structural growth sequences and electronic properties of zinc oxide clusters $(ZnO)_n$ (n=2−18). *J. Phys. Chem. C* **2007**, *111*, 4956−4963.
(39) Francisco, E.; Martin Pendas, A.; Blanco, M. A. Global optimization of ionic Mg_nF_{2n} (n=1−30) clusters. *J. Chem. Phys.* **2005**, DOI: 23430510.1063/1.2138688.
(40) Neelamraju, S.; Schon, J. C.; Doll, K.; Jansen, M. Ab initio and empirical energy landscapes of $(MgF_2)_n$ clusters (n=3, 4). *Phys. Chem. Chem. Phys.* **2012**, *14*, 1223−1234.
(41) Neelamraju, S.; Bach, A.; Schon, J. C.; Fischer, D.; Jansen, M. Experimental and theoretical study on Raman spectra of magnesium fluoride clusters and solids. *J. Chem. Phys.* **2012**, DOI: 19431910.1063/1.4765700.
(42) Woodley, S. M.; Hamad, S.; Mejias, J. A.; Catlow, C. R. A. Properties of small TiO_2, ZrO_2 and HfO_2 nanoparticles. *J. Mater. Chem.* **2006**, *16*, 1927−1933.
(43) Hamad, S.; Catlow, C. R. A.; Woodley, S. M.; Lago, S.; Mejias, J. A. Structure and stability of small TiO_2 nanoparticles. *J. Phys. Chem. B* **2005**, *109*, 15741−15748.
(44) Zhang, W. W.; Han, Y.; Yao, S. Y.; Sun, H. Q. Stability analysis and structural rules of titanium dioxide clusters $(TiO_2)_n$ with n=1−9. *Mater. Chem. Phys.* **2011**, *130*, 196−202.
(45) Marom, N.; Kim, M.; Chelikowsky, J. R. Structure selection based on high vertical electron affinity for TiO_2 clusters. *Phys. Rev. Lett.* **2012**, DOI: 10680110.1103/PhysRevLett.108.106801.
(46) Qu, Z. W.; Kroes, G. J. Theoretical study of stable, defect-free $(TiO_2)_n$ nanoparticles with n=10−16. *J. Phys. Chem. C* **2007**, *111*, 16808−16817.
(47) Calatayud, M.; Maldonado, L.; Minot, C. Reactivity of $(TiO_2)_N$ clusters (N=1−10): probing gas-phase acidity and basicity properties. *J. Phys. Chem. C* **2008**, *112*, 16087−16095.
(48) Woodley, S. M.; Hamad, S.; Catlow, C. R. A. Exploration of multiple energy landscapes for zirconia nanoclusters. *Phys. Chem. Chem. Phys.* **2010**, *12*, 8454−8465.
(49) Rahane, A. B.; Deshpande, M. D.; Kumar, V. Structural and electronic properties of $(Al_2O_3)_n$ clusters with n=1−10 from first principles calculations. *J. Phys. Chem. C* **2011**, *115*, 18111−18121.
(50) Sierka, M.; et al. Unexpected structures of aluminum oxide clusters in the gas phase. *Angew. Chem., Int. Ed.* **2007**, *46*, 3372−3375.
(51) Woodley, S. M. Atomistic and electronic structure of $(X_2O_3)_n$ nanoclusters; n=1−5, X = B, Al, Ga, In and Tl. *Proc. R. Soc. A: Math. Phys. Eng. Sci.* **2011**, *467*, 2020−2042.
(52) Li, R.; Cheng, L. J. Structural determination of $(Al_2O_3)_n$ (n=1−7) clusters based on density functional calculation. *Comput. Theor. Chem.* **2012**, *996*, 125−131.
(53) Rahane, A. B.; Deshpande, M. D. Structural and electronic properties of neutral and ionic $(Ga_2O_3)_n$ clusters with n=1−10. *J. Phys. Chem. C* **2012**, *116*, 2691−2701.
(54) BelBruno, J. J.; Burnin, A. Small germanium sulfide clusters: mass spectrometry and density functional calculations. *Phys. Chem. Chem. Phys.* **2010**, *12*, 8557−8563.
(55) Walsh, A.; Woodley, S. M. Evolutionary structure prediction and electronic properties of indium oxide nanoclusters. *Phys. Chem. Chem. Phys.* **2010**, *12*, 8446−8453.
(56) Woodley, S. M.; Battle, P. D.; Gale, J. D.; Catlow, C. R. A. The prediction of inorganic crystal structures using a genetic algorithm and energy minimisation. *Phys. Chem. Chem. Phys.* **1999**, *1*, 2535−2542.
(57) Gale, J. D.; Rohl, A. L. The General Utility Lattice Program (GULP). *Mol. Simul.* **2003**, *29*, 291−341.
(58) Woodley, S. M. *Knowledge Led Master Code*, http://www.ucl.ac.uk/klmc/Software (accessed 2012).
(59) Zhao, J. J.; Xie, R. H. Genetic Algorithms for the Geometry Optimization of Atomic and Molecular Clusters. *J. Comput. Theor. Nanosci.* **2004**, *1*, 117−131.
(60) Woodley, S. M.; Catlow, C. R. A.; Battle, P. D.; Gale, J. D. The prediction of inorganic crystal framework structures using excluded regions within a genetic algorithm approach. *Chem. Commun.* **2004**, 22−23.
(61) Wang, Y. C.; Lv, J.; Zhu, L.; Ma, Y. M. CALYPSO: A method for crystal structure prediction. *Comput. Phys. Commun.* **2012**, *183*, 2063−2070.
(62) Lyakhov, A. O.; Oganov, A. R.; Stokes, H. T.; Zhu, Q. New developments in evolutionary structure prediction algorithm USPEX. *Comput. Phys. Commun.* **2013**, *184*, 1172−1182.
(63) Woodley, S. M. Engineering microporous architectures: combining evolutionary algorithms with predefined exclusion zones. *Phys. Chem. Chem. Phys.* **2007**, *9*, 1070−1077.
(64) Schon, J. C.; Jansen, M. First step towards planning of syntheses in solid-state chemistry: Determination of promising structure candidates by global optimization. *Angew. Chem., Int. Ed.* **1996**, *35*, 1287−1304.
(65) Sierka, M. Synergy between theory and experiment in structure resolution of low-dimensional oxides. *Prog. Surf. Sci.* **2010**, *85*, 398−434.

(66) Chen, M. Y.; Dixon, D. A. Tree Growth-Hybrid Genetic Algorithm for Predicting the Structure of Small (TiO2)(n), n=2−13, Nanoclusters. *J. Chem. Theory Comput.* **2013**, *9*, 3189−3200.
(67) Segall, M. D.; et al. First-principles simulation: ideas, illustrations and the CASTEP code. *J. Phys.: Condens. Matter* **2002**, *14*, 2717−2744.
(68) Kresse, G.; Furthmüller, J. Efficiency of ab-initio total energy calculations for metals and semiconductors using a plane-wave basis set. *Comput. Mater. Sci.* **1996**, *6*, 15.
(69) Dovesi, R.; et al. CRYSTAL: a computational tool for the ab initio study of the electronic properties of crystals. *Z. Kristallogr.* **2005**, *220*, 571−573.
(70) Valiev, M.; et al. NWChem: a comprehensive and scalable open-source solution for large scale molecular simulations. *Comput. Phys. Commun.* **2010**, *181*, 1477−1489.
(71) Havu, V.; Blum, V.; Havu, P.; Scheffler, M. Efficient O(N) integration for all-electron electronic structure calculation using numeric basis functions. *J. Comput. Phys.* **2009**, *228*, 8367−8379.
(72) Blum, V.; et al. Ab initio molecular simulations with numeric atom-centered orbitals. *Comput. Phys. Commun.* **2009**, *180*, 2175−2196.
(73) Schon, J. C.; Putz, H.; Jansen, M. Studying the energy hypersurface of continuous systems - The threshold algorithm. *J. Phys.: Condens. Matter* **1996**, *8*, 143−156.
(74) Woodley, S. M.; Walker, A. M. New software for finding transition states by probing accessible, or ergodic, regions. *Mol. Simul.* **2007**, *33*, 1229−1231.
(75) Dick, B. G.; Overhauser, A. W. Theory of the dielectric constants of alkali halide crystals. *Phys. Rev.* **1958**, *112*, 90.
(76) Valerio, M. E. G.; Jackson, R. A.; de Lima, J. F. Derivation of potentials for the rare-earth fluorides, and the calculation of lattice and intrinsic defect properties. *J. Phys. Condens. Matter* **2000**, *12*, 7727−7734.
(77) Perdew, J. P.; et al. Restoring the density-gradient expansion for exchange in solids and surfaces. *Phys. Rev. Lett.* **2008**, *100*, 136406−136404.
(78) Ernzerhof, M.; Scuseria, G. E. Assessment of the Perdew-Burke-Ernzerhof exchange-correlation functional. *J. Chem. Phys.* **1999**, *110*, 5029−5036.
(79) Vanlenthe, E.; Baerends, E. J.; Snijders, J. G. Relativistic total-energy using regular approximations. *J. Chem. Phys.* **1994**, *101*, 9783−9792.
(80) Hedin, L. New method for calculating 1-particle Greens function with application to electron-gas problem. *Phys. Rev.* **1965**, *139*, A796−+.
(81) Hybertsen, M. S.; Louie, S. G. 1st-principles theory of quasiparticles - calculation of band-gaps in semiconductors and insulators. *Phys. Rev. Lett.* **1985**, *55*, 1418−1421.
(82) Jiang, H.; Gomez-Abal, R. I.; Rinke, P.; Scheffler, M. Localized and itinerant states in lanthanide oxides united by GW @ LDA plus U. *Phys. Rev. Lett.* **2009**, DOI: 12640310.1103/PhysRevLett.102.126403.
(83) Rinke, P.; Janotti, A.; Scheffler, M.; Van de Walle, C. G. Defect formation energies without the band-gap problem: combining density-functional theory and the GW approach for the silicon self-interstitial. *Phys. Rev. Lett.* **2009**, DOI: 02640210.1103/PhysRevLett.102.026402.
(84) Herzberg, G. *Atomic spectra and atomic structure*; Dover: New York, 1944.
(85) Banerjee, A.; Adams, N.; Simons, J.; Shepard, R. Search for stationary-points on surface. *J. Phys. Chem.* **1985**, *89*, 52−57.
(86) Metropolis, N.; Rosenbluth, A. W.; Rosenbluth, M. N.; Teller, A. H.; Teller, E. Equations of state calculations by fast computing machines. *J. Chem. Phys.* **1953**, *21*, 1087−1092.
(87) Keal, T. W.; Sherwood, P.; Dutta, G.; Sokol, A. A.; Catlow, C. R. A. Characterization of hydrogen dissociation over aluminium-doped zinc oxide using an efficient massively parallel framework for QM/MM calculations. *Proc. R. Soc. A: Math. Phys. Eng. Sci.* **2011**, *467*, 1900−1924.
(88) Xu, W.; Ji, W. X.; Qiu, Y. X.; Schwarz, W. H. E.; Wang, S. G. On structure and bonding of lanthanoid trifluorides LnF_3 (Ln = La to Lu). *Phys. Chem. Chem. Phys.* **2013**, *15*, 7839−7847.
(89) Weigand, A.; Cao, X.; Yang, J.; Dolg, M. Quasirelativistic f-in-core pseudopotentials and core-polarization potentials for trivalent actinides and lanthanides: molecular test for trifluorides. *Theor. Chem. Acc.* **2010**, *126*, 117−127.
(90) Wiemhofer, H. D.; Harke, S.; Vohrer, U. Electronic-properties and gas interaction of LaF_3 and ZrO_2. *Solid State Ionics* **1990**, *40−1*, 433−439.
(91) Olson, C. G.; Piacentini, M.; Lynch, D. W. Optical-properties of single-crystals of some rare-earth trifluorides, 5−34-eV. *Phys. Rev. B* **1978**, *18*, 5740−5749.
(92) Krupa, J. C.; Gerard, I.; Martin, P. Vacuum UV excitation of luminescent materials by synchrotron radiation electronic-structure. *J. Alloys Compd.* **1992**, *188*, 77−81.
(93) Radzhabov, E.; Nepomnyashikh, A. I. In Proceedings of the 13th International Conference on Defects in Insulating Materials - Icdim 96- *Mater. Sci. Forum*; Matthews, G. E., Williams, R. T., Eds.; Trans Tech Publications Ltd.: Switzerland, 1997; Vol. *239*, pp 275−278.
(94) Sokol, A. A.; et al. On the problem of cluster structure diversity and the value of data mining. *Phys. Chem. Chem. Phys.* **2010**, *12*, 8438−8445.